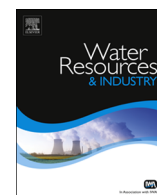


Contents lists available at [ScienceDirect](http://ScienceDirect)

# Water Resources and Industry

journal homepage: [www.elsevier.com/locate/wri](http://www.elsevier.com/locate/wri)

## Kinetics, isotherms and thermodynamic modeling of liquid phase adsorption of Rhodamine B dye onto *Raphia hookerie* fruit epicarp

A.A. Inyinbor<sup>a,b,\*</sup>, F.A. Adekola<sup>b</sup>, G.A. Olatunji<sup>b</sup><sup>a</sup> Department of Physical Sciences, Landmark University, P.M.B 1001 Omu Aran, Nigeria<sup>b</sup> Department of Industrial Chemistry, University of Ilorin, P.M.B 1515 Ilorin, Nigeria

### ARTICLE INFO

#### Article history:

Received 19 November 2015

Received in revised form

10 June 2016

Accepted 13 June 2016

#### Keywords:

*Raphia hookerie*

Biomass

Rhodamine B

Adsorption

Thermodynamics

Kinetics

### ABSTRACT

Highly efficient low cost adsorbent was prepared from *Raphia hookerie* fruit epicarp. Characteristics of the prepared low cost adsorbent (RH) was established using scanning electron microscope (SEM), Fourier Transform Infra Red (FTIR) and Brunauer–Emmett–Teller (BET) surface area. RH was applied for Rhodamine B (RhB) uptake from aqueous solution. Equilibrium adsorption data were fitted using four isotherms and kinetic data tested with five kinetic models. The BET surface area obtained was 0.00351 m<sup>2</sup>/g; SEM reveals large pores that could enhance the uptake of large molecules. Freundlich isotherm best described the uptake of RhB onto RH, the maximum monolayer adsorption capacity ( $q_{\max}$ ) was 666.67 mg/g. Pseudo second order model best described the kinetics of adsorption process. Energy of adsorption (E) obtained from D-R isotherm suggests physical adsorption. Desorption efficiency follows the order H<sub>2</sub>O > HCl > CH<sub>3</sub>COOH. Cost analysis shows that RH is about 1143 times more economical when compared with commercial activated carbon.

© 2016 Elsevier B.V. This is an open access article under the CC BY-NC-ND license (<http://creativecommons.org/licenses/by-nc-nd/4.0/>).

## 1. Introduction

Textile industries generate large volume of wastewater that majorly emanate from the dye preparation, spent dye, bath and washing stages. This wastewater usually contains loads of dye molecules that are hazardous, thereby posing threats to human and other living organisms in the environment [1]. Textile industries utilize varieties of dyes such as anthraquinone based meta complex, reactive, acidic, azo, diazo, and basic. While dyeing of wool, silks, acrylic and nylon is commonly done using basic dyes, reactive dyes are better employed in other industrial dyeing processes [2]. Dyes are characterized by high molecular weight and complex chemical structures; hence, they are non-biodegradable [3].

Conventional methods of effluents treatments such as precipitation, electrochemical treatment, reverse osmosis, ion exchange, evaporation, solvent extraction, as well as adsorption with activated charcoal among others; are presently in use for the treatment of textile industrial effluent. Adsorption with activated carbon has been found to be effective because of the simplicity in its design and operation, ability to adsorb a broad range of pollutants; and fast adsorption kinetics [4]. However, the commercial activated carbon is very expensive due to the high cost of precursor, hence the quest for a more economical way of textile effluent treatment [5]. Investigations into the use of low cost adsorbent, especially bioresource

\* Corresponding author at: Department of Physical Sciences, Landmark University, P.M.B 1001 Omu Aran, Nigeria.

E-mail addresses: [inyinbor.adejumoke@landmarkuniversity.edu.ng](mailto:inyinbor.adejumoke@landmarkuniversity.edu.ng), [adejumokebose@yahoo.com](mailto:adejumokebose@yahoo.com) (A.A. Inyinbor), [fadekola@unilorin.edu.ng](mailto:fadekola@unilorin.edu.ng) (F.A. Adekola).

<http://dx.doi.org/10.1016/j.wri.2016.06.001>

2212-3717/© 2016 Elsevier B.V. This is an open access article under the CC BY-NC-ND license (<http://creativecommons.org/licenses/by-nc-nd/4.0/>).

materials as an alternative to commercial activated carbon do not only give economical advantage, it also aids environmental protection and encourages waste management. Waste materials, which naturally would have been nuisance to the environment; become useful environmental remediation tools. Lignocellulosic materials such as agricultural wastes have cellulose, hemicellulose and lignin as their basic constituents. Their polyol backbone coupled with the presence of other functional groups serve as good binding site for pollutants. Although, surface modification or functionalization may result into adsorbents with superior adsorption capacity, this however also results in decreased economic advantages [6].

Investigations into the use of various wastes as alternative low cost adsorbent for the treatment of synthetic textile industrial effluents have been widely reported. Investigation into the use of Cupuassu shells in the uptake of reactive red and direct blue dyes has been reported. Uptake of dye was more favorable in the acidic media, and equilibrium data was reported to fit best into the Sip isotherm model [7]. Removal of Ramazol black textile dye using pine fruit shell was also investigated, and reported. Acidic media also favoured the uptake of Ramazol black onto pine fruit shells, while equilibrium adsorption data fitted best into the Sip isotherm model [8]. Bello et al. [9] reported the use of ackee apple seeds in the removal of Congo Red dye from aqueous solution. Optimum adsorption was observed at pH 3. Adsorption process was fast and equilibrium was attained within 90 min. The equilibrium adsorption data fitted best into the Langmuir isotherm model. Seed husk of bangal gram was utilized for the removal of congo red, adsorption data obtained were analyzed using Langmuir isotherm, and  $q_{\max}$  obtained was 41.66 mg/g [10]. Removal of Methylene blue and Eriochrome black T using Maize stem tissue has been investigated and reported. Maximum monolayer adsorption capacities were reported to be 160.84 mg/g and 167.01 mg/g for methylene blue and eriochrome black T respectively. Equilibrium adsorption data for the two dyes, was described by Freundlich and Langmuir isotherm models [11]. The use of dika nut endocarp waste in the uptake of Rhodamine B has also been recently reported. Optimum adsorption was obtained at pH 3, equilibrium adsorption data fitted best into the Freundlich adsorption isotherm, and maximum monolayer adsorption capacity was obtained to be 212.77 mg/g [12].

*Raphia hookerie* belongs to the *Palmicea* family. Members of this family contain high cellulosic fibers, are good source of carbon, and have been found suitable in activated carbon preparation [13]. While other members of this family have been well explored in activated carbon preparation as well as effective low cost adsorbent [14–18], *Raphia hookerie* have been neglected. To the best of our knowledge, *Raphia hookerie* epicarp is yet to find applications in environmental remediation. This study therefore aimed at investigating the potential of low cost adsorbent prepared from the epicarp of *Raphia hookerie* fruit in the adsorption of a cationic dye (Rhodamine B- RhB). The physicochemical characteristics, functional groups analysis, and surface morphology of the prepared adsorbents were studied. Studies on the adsorption capacity of the biomaterial viz-a-viz kinetics, isotherms and thermodynamics analysis of the adsorption data, were carried out. The modes and mechanism of RhB uptake were well investigated and the kinetics models were validated using statistical tools. Economic advantage of the prepared adsorbent over modified biomass and commercial activated carbon are also presented.

## 2. Materials and methods

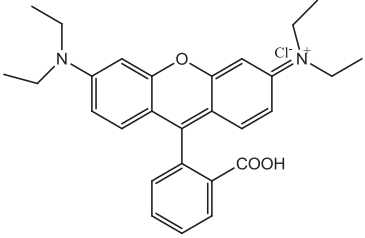
### 2.1. Adsorbent preparation

Epicarp of *Raphia hookerie* fruits were collected from local farmers in Mokogi, Edu Local Government Area of Kwara State, Nigeria. In order to remove dirt, the biomass was washed with abundant water and dried in an oven operated at 105 °C



Fig. 1. Raw *Raphia hookerie* fruit.

**Table 1**  
Properties of Rhodamine B.

Parameters	Values
Suggested name	Rhodamine B
C.I number	45170
C.I name	Basic violet 10
Class	Rhodamine
$\lambda_{\max}$	554nm
Molecular formular	$C_{28}H_{31}N_2O_3Cl$
Molecular weight	479.02
Chemical structure	

overnight. It was then pulverized and screened into a particle size of 150–250  $\mu\text{m}$ . It was washed, dried and stored in a closed container. Fig. 1 shows the *Raphia hookerie* fruits.

## 2.2. Characterization of the adsorbent

The topography and the elemental composition of the adsorbent were studied using a FEIESEM quanta 200 for SEM and EDX. The surface area, pore volume and pore size were obtained using a micrometric Tristar II surface area and porosity analyser. Various functional groups present on the surfaces of the adsorbents were studied using a Bruker ALPHA FTIR spectrophotometer.

## 2.3. Preparation of Rhodamine B (RhB) solution

RhB, with properties listed in Table 1 was supplied by BDH; 1000 mg/L RhB solution was prepared by dissolving accurately weighed samples of RhB in 1 l of deionized water. Serial dilution was done to obtain other desired lower concentrations.

## 2.4. Batch kinetics and equilibrium adsorption studies

Certain parameters greatly affects the adsorption process [19], thus, batch adsorption studies with respect to initial solution pH (pH 2–9), initial RhB concentration and contact time (50–400 mg/L), adsorbent dosage (1–5 g/L) and temperature (303–333 K) on the removal of RhB were carried out. The pH of the RhB solution was adjusted by adding 0.1 M HCl or 0.1 M NaOH. In each adsorption experiment, 0.1 g of the adsorbent (RH) was added to 100  $\text{cm}^3$  samples of RhB solution of a specific concentration in a 250  $\text{cm}^3$  glass conical flask. The flask was agitated for 50 min in a thermostated water bath shaker operated at 26  $^\circ\text{C}$  and 130 rpm to reach equilibrium. Then the adsorbent was separated from solution by centrifugation. The concentration of unadsorbed dye was determined using a Beckman Coulter Du 730 UV/vis spectrophotometer at 554 nm. Quantity adsorbed at a given time  $t$  was calculated using Eq. (1) and percentage removal was obtained using Eq. (2):

$$q_t = \frac{(C_i - C_t)}{M} \times V \quad (1)$$

$$\% \text{Removal} = \frac{(C_i - C_t)}{C_i} \times 100 \quad (2)$$

where  $C_i$ ,  $C_t$  and  $C_f$  are the initial RhB concentration, the concentration of RhB at time  $t$  and final concentration of RhB respectively.  $V$  is the volume of RhB solution used for the adsorption studies in liter and  $M$  is the weight of the adsorbent in g.

## 2.5. Mathematical modeling

### 2.5.1. Isothermal studies

At the equilibrium of an adsorption process, adsorption isotherm is suitable in describing the distribution of adsorbate molecules between the liquid and the solid phase [20]. Four adsorption isotherms viz: the Langmuir, Freundlich, Temkin and Dubinin–Radushkevich (D–R) models were used to analyze the adsorption data. Important information such as adsorption mechanism, favorability of adsorption process and adsorbate-adsorbent affinity may be obtained. The Langmuir isotherm [21] which assumes a surface with homogeneous binding sites, equivalent sorption energies, and no interactions between adsorbed species is expressed by the mathematical relation (3);

$$\frac{C_e}{q_e} = \frac{C_e}{q_{max}} + \frac{1}{q_{max}K_L} \quad (3)$$

where  $C_e$  is the equilibrium concentration of RhB dye (mg/L),  $q_e$  is the quantity of RhB dye adsorbed onto the adsorbent at equilibrium (mg/g),  $q_{max}$  is the maximum monolayer adsorption capacity of adsorbent (mg/g) and  $K_L$  is the Langmuir adsorption constant (L/mg). The plot of  $C_e/q_e$  against  $C_e$  gives a straight line with a slope and intercept of  $1/q_{max}$  and  $1/q_{max}K_L$  respectively.  $K_L$  is an important tool in the calculation of the dimensionless equilibrium parameters ( $R_L$ ) that explains the favorability of adsorption process;  $R_L$  is calculated using Eq. (4).

$$R_L = \frac{1}{(1 + K_L C_0)} \quad (4)$$

The Freundlich isotherm [22] that is an empirical model not limited to monolayer coverage alone but also describe multilayer adsorption. It is expressed mathematically as;

$$\log q_e = \frac{1}{n} \log C_e + \log K_f \quad (5)$$

where  $q_e$  is the quantity of RhB adsorbed at equilibrium (mg/g),  $C_e$  is the concentration (mg/L) of RhB in solution at equilibrium;  $K_f$  and  $n$  are Freundlich constants incorporating the factors affecting the adsorption capacity and adsorption intensity respectively. The Plots of  $\log q_e$  against  $\log C_e$  gives a linear graph with slope  $1/n$  and intercept  $\log K_f$  from which  $n$  and  $K_f$  can be calculated respectively.

Dubinin Radushkevich (D-R) model is a more general model in which assumption is not based on homogenous surface or constant adsorption potential, it gives insight into the biomass porosity as well as the adsorption energy. The value of adsorption energy further provides information as to whether adsorption process is physical or chemical in nature [23]. D-R model is expressed mathematically by Eq. (6);

$$\ln q_e = \ln q_0 - \beta \epsilon^2 \quad (6)$$

where  $q_e$  is the amount of RhB ions adsorbed per unit weight of adsorbent (mg/g),  $q_0$  is the maximum adsorption capacity,  $\beta$  is the activity coefficient useful in obtaining the mean sorption energy  $E$  (kJ/mol) and  $\epsilon$  is the Polanyi potential.  $\epsilon$  and  $E$  are expressed by Eqs. (6a) and (6b) respectively;

$$\epsilon = RT \ln \left( 1 + \frac{1}{C_e} \right) \quad (6a)$$

$$E = \sqrt{1}/2\beta \quad (6b)$$

where  $R$  is the gas constant (J/mol K) and  $T$  is the temperature (K).  $q_0$  and  $\beta$  ( $\text{mol}^2/\text{kJ}^2$ ) can respectively be calculate from the intercept and the slope of the plot of  $\ln q_e$  vs  $\epsilon^2$ .

The Temkin isotherm assumes linear rather than logarithm decrease of heat of adsorption while ignoring extremely low and very high concentration. It also assumes uniform distribution of bounding energy up to some maximum bonding energy. It is expressed by Eq. (7) below [24].

$$q_e = B \ln A + B \ln C_e \quad (7)$$

where  $q_e$  is the amount of adsorbate adsorbed at equilibrium (mg/g);  $C_e$  is concentration of adsorbate in solution at equilibrium (mg/L).  $B$  is a constant related to the heat of adsorption and it is defined by the expression  $B = RT/b$ ,  $b$  is the Temkin constant (J/mol),  $T$  is the absolute temperature (K),  $R$  is the gas constant (8.314 J/mol K), and  $A$  is the Temkin isotherm constant (L/g). From the plot of  $q_e$  vs.  $\ln C_e$ ,  $B$  and  $A$  can be calculated from the slopes ( $B$ ) and intercepts ( $B \ln A$ ) respectively.

### 2.5.2. Kinetics model

The possible dye adsorption mechanism as well as possible rates controlling steps may be established via kinetics models [25]. The kinetic of the adsorption systems were studied using the pseudo-first-order, pseudo-second-order, Elovich, Avrami and fractional power models. The intraparticle diffusion and Bangham models investigated the mechanism of adsorption.

The pseudo first-order kinetic model of Lagergren [26] given by the equation;

$$\ln(q_e - q_t) = \ln q_e - k_1 t \quad (8)$$

where  $q_e$  is the quantity adsorbed at equilibrium (mg/g) and  $q_t$  is the quantity adsorbed at time  $t$  (mg/g).  $k_1$  is the rate constant for the pseudo-first-order sorption ( $\text{min}^{-1}$ ). A linear graph with negative slope is expected from the plot of  $\ln(q_e - q_t)$  against  $t$  at different concentrations,  $k_1$  and  $q_{cal}$  can then be obtained from the slope and intercept respectively.

The pseudo-second-order kinetic model [27], presented in Eq. (9);

$$t/q_t = 1/k_2 q_e^2 + 1(t)/q_e \quad (9)$$

where  $K_2$  is the rate constant of the pseudo-second-order kinetic equation in  $\text{g/mg min}^{-1}$ ,  $q_e$  is the maximum sorption capacity in mg/g and  $q_t$  (mg/g) is the amount of sorption at time  $t$ . Linear graphs are obtained from a plot of  $t/q_t$  against  $t$  from which  $q_e$  and  $k_2$  can be calculated from the slope and intercepts.

The Elovich kinetic model in its nonlinear and linear form is expressed by the (Eqs. (10) and 11) respectively [28].

$$q_t = \beta \ln(\alpha \beta t) \quad (10)$$

$$q_t = 1/\beta \ln(\alpha \beta) + 1/\beta \ln t \quad (11)$$

where  $q_t$  is the quantity of adsorbate adsorbed at time  $t$  (mg/g),  $\alpha$  is a constant related to chemisorption rate and  $\beta$  is a constant which depicts the extent of surface coverage. The two constants ( $\alpha$  and  $\beta$ ) can be calculated from the intercept and slope of the plot of  $q_t$  versus  $\ln t$  respectively.

(Eqs. (12) and 13) express the non linear and linear forms of Avrami kinetic model respectively [29].

$$q_t = q_e \left\{ 1 - \exp \left[ - (K_{Av} t)^{n_{Av}} \right] \right\} \quad (12)$$

$$\ln[-\ln(1-\alpha)] = n_{Av} K_{Av} + n_{Av} \ln t \quad (13)$$

$K_{Av}$  is the Avrami constant and  $n_{Av}$  is the Avrami model exponent of time related to the change in mechanism of adsorption.  $K_{Av}$  and  $n_{Av}$  can be obtained from the intercept and slope of the plot of  $\ln[-\ln(1-\alpha)]$  against  $\ln t$ .

The nonlinear and linear forms of Fractional power kinetic model equation are depicted by (Eqs. (14) and 15) respectively;

$$q_t = K t^v \quad (14)$$

$$\log q_t = \log K + v \log t \quad (15)$$

$\log K$  and  $v$  are the intercept and slope of the plot of  $\log q_t$  versus  $\log t$  respectively thus antilog of intercept gives the value of constant  $k$ .  $v$  is also a constant that is usually less than unity if adsorption kinetic data fits well into power function model.  $q_t$  is the quantity of adsorbate adsorbed at time  $t$ .

**2.5.2.1. Validation of adsorption kinetics.** Chi square and the normalized standard deviation given by the (Eqs. (16) and 17) were used to validate the kinetics model.

$$\chi^2 = \sum_{i=1}^n \frac{(q_{exp} - q_{cal})^2}{q_{cal}} \quad (16)$$

$$\Delta q_e(\%) = 100 \sqrt{\left[ \frac{(q_{exp} - q_{cal})/q_{exp}}{N-1} \right]} \quad (17)$$

where  $N$  is the number of data points while  $q_{exp}$  and  $q_{cal}$  are experimentally determined quantity adsorbed at equilibrium and calculated quantity adsorbed at equilibrium respectively.

### 2.5.3. Adsorption mechanism

The intraparticle diffusion model by Weber and Morris [30] expressed by the mathematical relation in Eq. (18);

$$q_t = K_{diff} t^{1/2} + C \quad (18)$$

where  $q_t$  ( $\text{mg g}^{-1}$ ) is the amount of RhB dye adsorbed at time  $t$  and  $K_{diff}$  ( $\text{mg g}^{-1} \text{min}^{-1/2}$ ) is the rate constant for intraparticle diffusion. Insight into the thickness of the boundary layer can be obtained from the value of  $C$ , large intercept suggests great boundary layer effect. A plot of  $q_t$  versus  $t^{0.5}$  can give a linear or multilinear suggesting that intraparticle diffusion is involved in the adsorption process or two or more steps govern the adsorption process. However, if a linear graph is obtained and the plot passes through the origin then intraparticle diffusion is said to be the sole rate-limiting step.

Adsorbate pore diffusion activities were investigated using the Bangham models;

$$\text{Log } \log \left( \frac{C_i}{C_i - q_t M} \right) = \log \left( \frac{K_j M}{2.303 V} \right) + \alpha \log t \quad (19)$$

where  $C_i$  is the initial concentration of dye solution (mg/L),  $V$  is the volume of dye solution in mL,  $M$  is the mass of adsorbent (g/L),  $q_t$  is the quantity of dye adsorbed at time  $t$  and  $\alpha$  ( $< 1$ ) and  $K_j$  are constants which can be obtained from slope and intercept respectively.

#### 2.5.4. Thermodynamic studies

Effects of temperature on the uptake of RhB onto RH was studied, thermodynamic parameters that explains feasibility, spontaneity and the nature of adsorbate-adsorbent interactions ( $\Delta G^\circ$ ,  $\Delta H^\circ$  and  $\Delta S^\circ$ ) were calculated using the mathematical relations (20) and (21);

$$\ln K_o = \frac{\Delta S^\circ}{R} - \frac{\Delta H^\circ}{RT} \quad (20)$$

$$\Delta G^\circ = -RT \ln K_o \quad (21)$$

where  $T$  is the temperature in Kelvin,  $R$  is the gas constant and  $K_o$  can be obtained from  $q_e/C_e$ . A plot of  $\ln K_o$  versus  $1/T$  should give a linear plot and  $\Delta H^\circ$  and  $\Delta S^\circ$  can be calculated from the slope and intercept respectively.

#### 2.6. Desorption of RhB from RH

Mechanism of pollutant uptake as well as reusability of adsorbent can be better understood via desorption experiments. Leaching/desorption of RhB from RH was investigated using deionized water, 0.1 M HCl and 0.1 M  $\text{CH}_3\text{COOH}$ . Fresh adsorbent was loaded with RhB by agitating mixture of 0.1 g and  $100 \text{ cm}^3$  of 100 mg/L RhB solution at pH 3.0 for 1 h. The RhB-loaded adsorbents were separated by centrifugation and the residual RhB concentration determined spectrophotometrically. The RhB loaded adsorbents were washed gently with water to remove any unadsorbed dye and dried. The desorption process was carried out by mixing  $100 \text{ cm}^3$  of each desorbing eluent with the dried loaded-adsorbents and shaken for a predetermined time and the desorbed RhB was determined spectrophotometrically. Desorption efficiency was calculated using the mathematical relation below;

$$\text{Desorption efficiency}(\%) = \frac{q_{de}}{q_{ad}} \times 100 \quad (22)$$

where  $q_{de}$  is the quantity desorbed by each of the eluent and  $q_{ad}$  is the adsorbed quantity during loading.

### 3. Results and discussion

#### 3.1. Adsorbents characterization

The topographies and morphologies of RH before and after RhB uptake are presented in Fig. 2. The surface of RH before

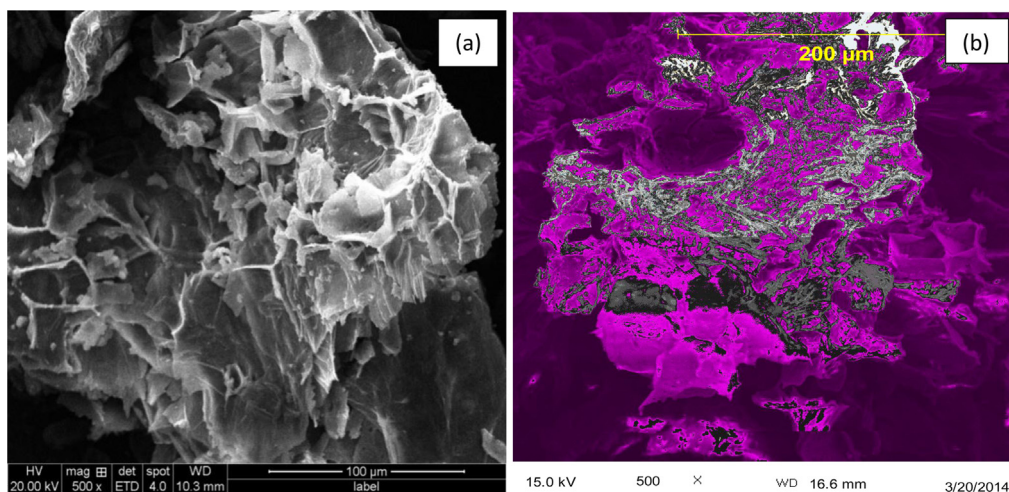


Fig. 2. Surface morphology of RH before RhB dye adsorption (a) and after RhB dye adsorption (b).



**Table 2**  
Characteristics of RH.

Parameters	Values RH
pH	5.75
PZC	5.80
Bulk density	0.26
Moisture content (%)	0.60
Ash content (%)	4.17
BET surface area ( $\text{m}^2/\text{g}$ )	0.0351
Average pore diameter ( $\text{\AA}$ )	< 0.001
Elemental composition (%)	
Carbon	69.93
Oxygen	29.66
Potassium	0.41

adsorption was observed to have large leather like open pores (Fig. 2(a)), however the surface was observed to be rough after RhB uptake. The surface area of RH was observed to be low (Table 2), due to various functional groups which occupies the surface area of agricultural waste, they are usually characterized by low surface area [31,32]. The affinity of the adsorbent for water was found to be low with percentage moisture content of 0.60% and high carbon content suggests that the adsorbent will be suitable in the uptake of pollutants.

The surface functional groups of the adsorbent were established using FTIR. The FTIR spectra of RH before and after dye adsorption are shown in Fig. 3. Vivid absorption band at  $1029.95 \text{ cm}^{-1}$  corresponds to C-OH stretching, while the other absorption occurring at  $1239.09 \text{ cm}^{-1}$ ,  $1729.93 \text{ cm}^{-1}$ ,  $2919.82 \text{ cm}^{-1}$ ,  $1424.27 \text{ cm}^{-1}$  and  $3297.82 \text{ cm}^{-1}$  corresponds to C-N stretching vibrations, C=O of amide, C-H stretching vibrations,  $\text{CH}_3$  bending and O-H of alcohol respectively. The shift of the various absorption bands to a higher or lower frequency after dye adsorption (Table 3) shows that these functional groups participated in the uptake of RhB. After RhB adsorption, new peak was also observed at around  $1600 \text{ cm}^{-1}$  which corresponds to aromatic ring vibration.

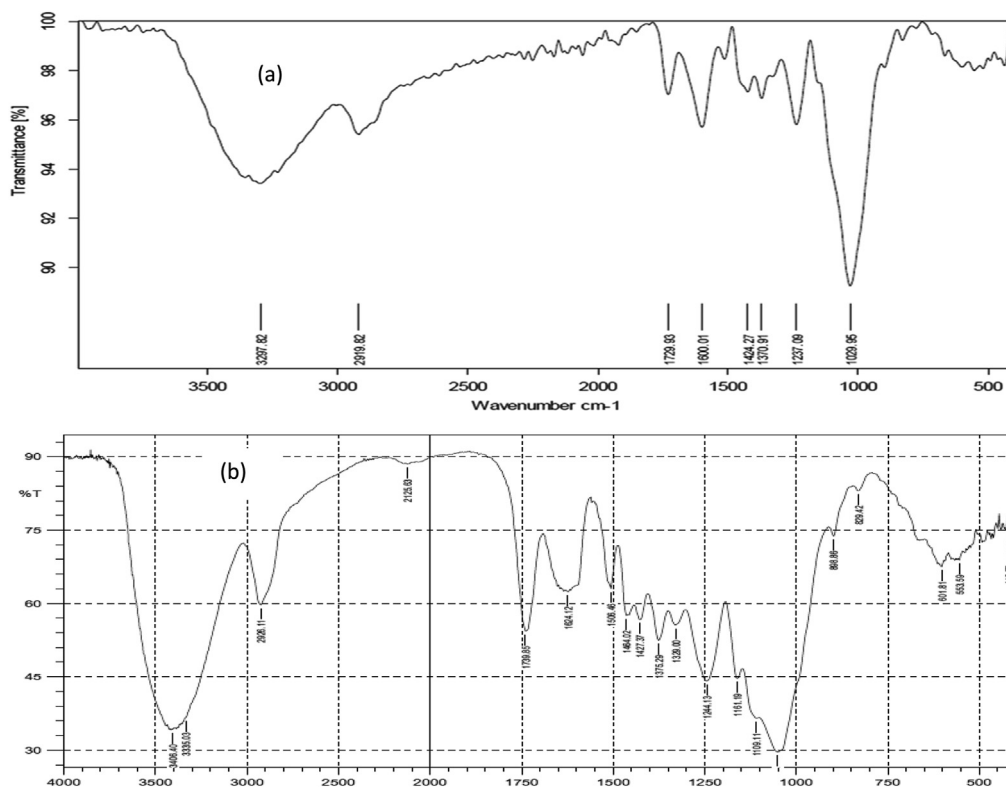


**Fig. 3.** FTIR spectral of RH (a) before RhB adsorption (b) after RhB adsorption.

**Table 3**  
FTIR spectral characteristics of RH before and after RhB adsorption.

Assignment for IR peak	Wave number ( $\text{cm}^{-1}$ )		
	RH		
	Before adsorption	After adsorption	Differences
C–OH stretching	1029	1051	22
C–N stretching	1237	1244	7
C=O of amide	1729	1739	10
C–H stretching	2919	2926	7
O–H stretching	3297	3335	8

### 3.2. Effects of pH

The pH of the solution greatly influences adsorption process; it determines the surface charge of the adsorbent and the state of adsorbate in solution. pH effects on the uptake of RhB onto RH was investigated and the highest percentage RhB uptake was obtained at pH 3 (Fig. 4). Rapid adsorption was observed between pH 2 and 3 while percentage adsorption decreased gradually above pH 3. RhB with pka of 3.7 may exists as cationic, lactonic or zwitterionic form depending on the solution media. Zwitterionic form of RhB dominates at pH greater than that of RhB pka hence attraction between the xanthene and the carboxyl groups of RhB monomers occurs resulting into RhB dimers and subsequently a decrease in RhB adsorption [33]. Optimum adsorption at pH of 3 has been previously reported by researchers [34]. Subsequent adsorption studies were carried out at the optimum pH.

### 3.3. Effects of initial concentration and contact time

Fig. 5 depict the effects of concentration and contact time on RhB uptake onto RH. Quantity of RhB dye adsorbed was observed to increase with increased time and concentration, RhB uptake was rapid initially and gradually goes to equilibrium with increased time. Quantity adsorbed at equilibrium for initial RhB concentration of 50, 100, 200, 300 and 400 mg/L were 43.5, 85, 166.25, 243.75 and 312 mg/g respectively (Fig. 5). Rapid initial adsorption may be attributed to contacts of RhB molecules with available surface adsorption sites while subsequent gradual adsorption may be attributed to uptake of RhB molecules into the pores of the adsorbents. Equilibrium was attained at 40 min for initial dye concentration of 50, 200 and 400 mg/L and at 50 min for initial concentration of 100 and 300 mg/L.

### 3.4. Effects of adsorbent dosage

Percentage adsorbed was observed to increase as the adsorbent dosage increased and equilibrium was attained after adsorbent dosage of 2 g/L (Fig. 6). Percentage adsorbed increased from 85.19% for adsorbent dosage of 1 g/L to 88.88% for adsorbent dosage of 2 g/L. Increase in percentage adsorbed with increase in adsorbent dosage between 1 g/L and 2 g/L may be as a result of increase in the available adsorption sites. Only about 3% increase was observed as adsorbent dosage was increased from 1 g/L to 2 g/L, overlap of adsorption sites may account for the small increase in percentage adsorption. However, saturation viz-à-viz aggregation on adsorption site results into equilibrium after 2 g/L dosage (Fig. 7).

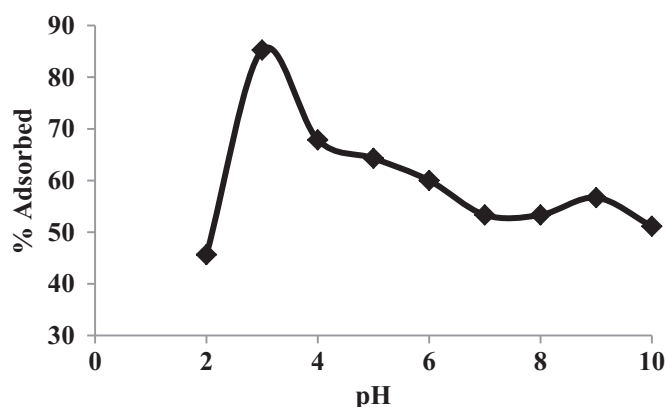


**Fig. 4.** pH effects on the percentage removal RhB uptake by RH [Dosage (1 g/L), agitation speed (130 rpm), agitation time (60 min), temperature (26 °C), initial Adsorbate concentration (100 mg/L)].



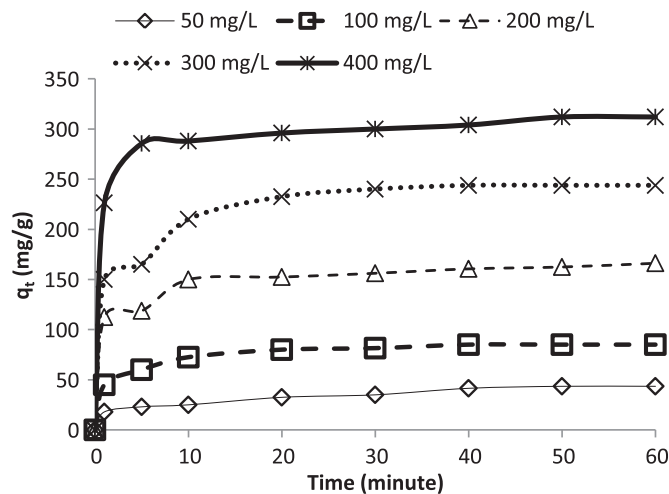


**Fig. 5.** Effects of contact time and initial dye concentration on RhB adsorption onto RH [Dosage (1 g/L), agitation speed (130 rpm), temperature (26 °C), pH (3)].

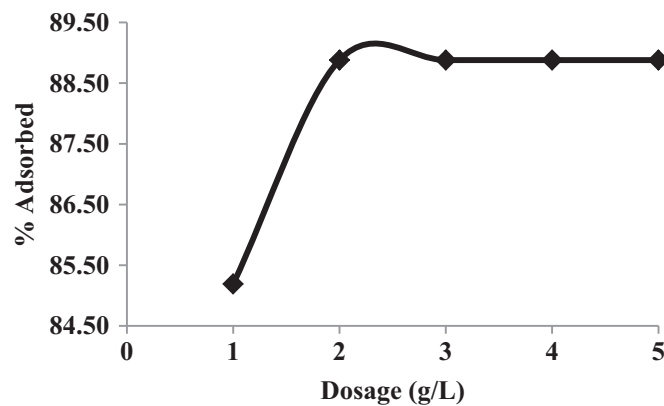


**Fig. 6.** Effects of adsorbent dosage on RhB adsorption onto RH [agitation speed (130 rpm), Initial concentration (100 mg/L), temperature (26 °C), pH (3)].

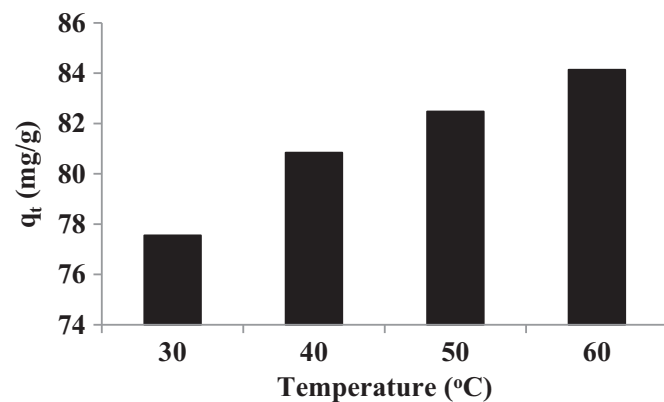


**Fig. 7.** Effects of temperature on the uptake of RhB onto RH. [Initial concentration (100 mg/L), agitation speed (130 rpm), adsorbent dosage (1 g/L), pH (3)].

### 3.5. Effects of temperature on the uptake of RhB onto RH

Quantity of RhB adsorbed was found to increase as temperature increased, quantity adsorbed increased from 77.55 to 84.14 mg/g as temperature increased from 30 to 60 °C. Increase in temperature may have generated energy required by large RhB specie to overcome activation barrier thus more RhB was able to penetrate the adsorbent RH. This study agrees with some reported works using Kaolinite and Montmorillonite [34].

**Table 4**

List of calculated parameters from the Langmuir, Freundlich, Temkin and D-R adsorption isotherm models.

Isotherms	constants	RH
Langmuir	$q_{\max}(\text{mg/g})$	666.67
	$K_L (\text{L mg}^{-1})$	0.01
	$R_L$	0.19
	$R^2$	0.9876
Freundlich	$K_f$	10.55
	$n$	1.29
	$R^2$	0.9969
	$B$	103.60
Temkin	$A (\text{L/g})$	0.19
	$b (\text{J/mol})$	24.08
	$R^2$	0.9600
	$q_o (\text{mg/g})$	208.38
D-R	$\beta (\text{mol}^2 \text{kJ}^{-2})$	0.01
	$E (\text{kJ mol}^{-1})$	6.11
	$R^2$	0.7900

### 3.6. Adsorption isotherm

Table 4 reports the various parameters obtained from the four isotherm plots. Calculated  $R_L$  value was less than 1 while the value of  $n$  was greater than 1 hence adsorption process was favorable. Freundlich isotherm best described the uptake of RhB onto RH ( $R^2$  value of 0.9969), this suggest that adsorption was not onto a uniform site rather a multilayer adsorption occurred in RhB-RH system. However, monolayer adsorption also played a very important role in the dye uptake onto RH ( $R^2$  for Langmuir is 0.9876). The maximum monolayer adsorption capacity for the uptake of RhB onto RH was obtained to be 666.67 mg/g, larger percentage of the adsorbed RhB molecules was recorded within the rapid adsorption (Section 3.3, Fig. 5). The Adsorption energy ( $E$ ) obtained from Dubinin–Radushkevich (D-R) isotherm was 6.11 kJ/mol suggesting that the uptake of RhB onto RH was by physisorption. Obtained maximum monolayer adsorption capacity ( $q_{\max}$ ) for the uptake of RhB onto RH has been compared with  $q_{\max}$  for other adsorbents available in the literatures (Table 5). RH apparently exhibits higher performance than other adsorbents earlier reported.

### 3.7. Adsorption kinetics

Calculated parameters of the various kinetics model and the validation results have been reported (Table 6). Low  $X^2$  and  $\Delta q_e$  characterized the pseudo second order and the Elovich models suggesting that these two models describe the kinetics of RhB uptake onto RH. The initial adsorption rate ( $h$ ) was found to increase as the initial adsorbate concentration increased suggesting that there was increase in driving force for mass transfer hence more dye molecule reached the adsorbent surface within a short period of time.  $\beta_{EI}$  is a constant related to the extension of surface coverage and decreased with increased in initial adsorbate concentration, the surface area of RH was obtained to be very low (Table 2) hence uptake of RhB onto RH may have been more through functional groups. However, the constant  $\alpha_{EI}$  that is related to chemisorption rate was found to increase as the initial dye concentration increased, this suggests that more than one mechanism governs the uptake of RhB onto RH [39]. Although the values of constant  $v$  obtained for the fractional power kinetic model was observed to be less than unity suggesting that fractional power may describe the adsorption kinetics of RhB-RH system. The large values of  $X^2$  and  $\Delta q_e$  obtained for fractional power and Avrami kinetic models validates that these two kinetic model does not describe the kinetics of RhB uptake onto RH. The Bangham and the intraparticle diffusion models clearly show that multiple adsorption stages occurred. Correlation coefficient obtained from the Bangham model ranged between 0.9069 and 0.9797 suggesting that pore diffusion was involved in RhB uptake onto RH. However, the linearity of the Bangham plot

**Table 5**Comparison of the maximum monolayer adsorption capacity ( $q_{\max}$ ) of RhB onto RH with others reported in literature.

Adsorbents	$q_{\max} (\text{mg/g})$	Ref
Modified coir pith	14.9	[35]
Bakers' yeast	25	[36]
Cedar Cone	4.55	[38]
Sugarcane baggase	51.5	[37]
Acid treated kaolinite	23.7	[34]
Acid treated montmorillonite	188.67	[34]
Raw dika nut waste	212.77	[12]
Acid treated dika nut waste	232.00	[12]
<i>Raphia hookerie</i> fruit epicarp	666.67	This study

**Table 6**

List of parameters obtained from Pseudo-first-order, Pseudo-second-order and intra particle diffusion kinetic model parameters for the adsorption of RhB onto RH.

Constants	Initial concentration				
	RH				
	50	100	200	300	400
<b>q<sub>e</sub> experimental (mg/g)</b>	43.50	85.00	166.25	243.75	312.00
<b>Pseudo first order</b>					
q <sub>e</sub> calculated (mg/g)	25.82	36.20	45.58	118.88	52.57
K <sub>1</sub> × 10 <sup>-2</sup> (min <sup>-1</sup> )	3.85	8.56	5.21	11.79	55.3
R <sup>2</sup>	0.9840	0.9520	0.9270	0.9960	0.7530
Δq <sub>e</sub>	2.36	4.71	7.53	3.75	9.88
X <sup>2</sup>	12.11	65.79	319.47	131.16	1280.27
<b>Pseudo second order</b>					
q <sub>e</sub> calculated (mg/g)	47.17	87.72	169.49	250.00	312.50
K <sub>2</sub> × 10 <sup>-3</sup> (g mg <sup>-1</sup> min <sup>-1</sup> )	3.37	6.37	3.70	2.39	3.94
h (mg g <sup>-1</sup> min <sup>-1</sup> )	6.38	46.02	102.27	141.99	383.54
R <sup>2</sup>	0.9820	0.9995	0.9991	0.9994	0.9994
Δq <sub>e</sub> (%)	10.20	2.00	0.50	0.90	3.66 × 10 <sup>-3</sup>
X <sup>2</sup>	0.2855	0.0843	0.0619	0.1563	0.0008
<b>Elovich</b>					
α <sub>EI</sub> (mg/g min)	55.23	858.87	34,178.07	6196.46	5627.62 × 10 <sup>3</sup>
β <sub>EI</sub> (g/mg)	0.1480	0.0970	0.07158	0.0379	0.0529
R <sup>2</sup>	0.9031	0.9745	0.9118	0.9274	0.9064
Δq <sub>e</sub> (%)	6.90	6.80	0.67	6.30	3.90
X <sup>2</sup>	0.068	0.11	2.17 × 10 <sup>-5</sup>	0.24	0.05
<b>Avrami</b>					
n <sub>Av</sub>	0.4191	0.4421	0.3222	0.441	0.2622
K <sub>av</sub> (min <sup>-1</sup> )	0.1368	0.4457	0.9652	0.5711	3.5677
R <sup>2</sup>	0.8322	0.9760	0.9067	0.8760	0.9545
Δq <sub>e</sub> (%)	34.99	35.05	35.22	35.24	35.28
X <sup>2</sup>	2064.16	4814.21	20,767.33	37,600.00	68,415.71
<b>Fractional power</b>					
V (min <sup>-1</sup> )	0.2315	0.1601	0.1019	0.1344	0.0704
K (mg/g)	16.57	46.83	110.38	147.03	238.34
KV (mg/g/min)	3.84	7.49	11.25	19.76	16.78
R <sup>2</sup>	0.9559	0.9612	0.9076	0.9264	0.8851
Δq <sub>e</sub>	34.69	34.95	35.12	35.18	35.21
X <sup>2</sup>	1075.52	3518.18	12,119.75	24,168.05	38,316.10
<b>Bangham</b>					
α	0.39	0.29	0.19	0.25	0.13
K <sub>1</sub> (g)	36.08	60.62	78.29	65.13	90.43
R <sup>2</sup>	0.9069	0.9797	0.9159	0.9311	0.9126
<b>Intra particle diffusion</b>					
C <sub>1</sub> × 10 <sup>2</sup> (mg g <sup>-1</sup> )	0.14	0.36	0.98	1.20	2.23
K <sub>i1</sub> (mg g <sup>-1</sup> min <sup>-1/2</sup> )	4.05	10.28	12.98	25.42	18.73
R <sub>1</sub> <sup>2</sup>	0.9730	0.9690	0.8420	0.9420	0.7350
C <sub>2</sub> × 10 <sup>2</sup> (mg g <sup>-1</sup> )	0.75	0.16	1.33	2.33	2.68
K <sub>i2</sub> (mg g <sup>-1</sup> min <sup>-1/2</sup> )	1.44	3.73	4.22	1.54	5.86
R <sub>2</sub> <sup>2</sup>	0.6460	0.8170	0.9820	0.6460	0.9100

suggests that adsorbate pore diffusion is not the only rate controlling step. Multilinear profile was obtained for intraparticle diffusion model plot and this plot did not pass through the origin (Fig. 8(f)), this suggests that boundary layer diffusion also occurred in the uptake of RhB onto RH. While k<sub>i1</sub>, C<sub>1</sub> and R<sub>1</sub><sup>2</sup> are the slope, intercept and correlation of the first steeper portion, k<sub>i2</sub>, C<sub>2</sub> and R<sub>2</sub><sup>2</sup> indicates the slope, intercept and correlation of the second linear portion respectively. Since the values of K<sub>i1</sub> are greater than the observed values of k<sub>i2</sub>, this indicates that intraparticle diffusion model mainly controlled the uptake of RhB onto RH.

### 3.8. Adsorption thermodynamics

Calculated thermodynamic parameters for the adsorption of RhB onto RH are reported on Table 7. Enthalpy (ΔH°) for RH-RhB system was positive suggesting that the adsorption process was endothermic in nature. ΔS° also was positive, (Table 7), suggesting that there was increase in the randomness at the solid-liquid interface during the adsorption of RhB onto RH, the

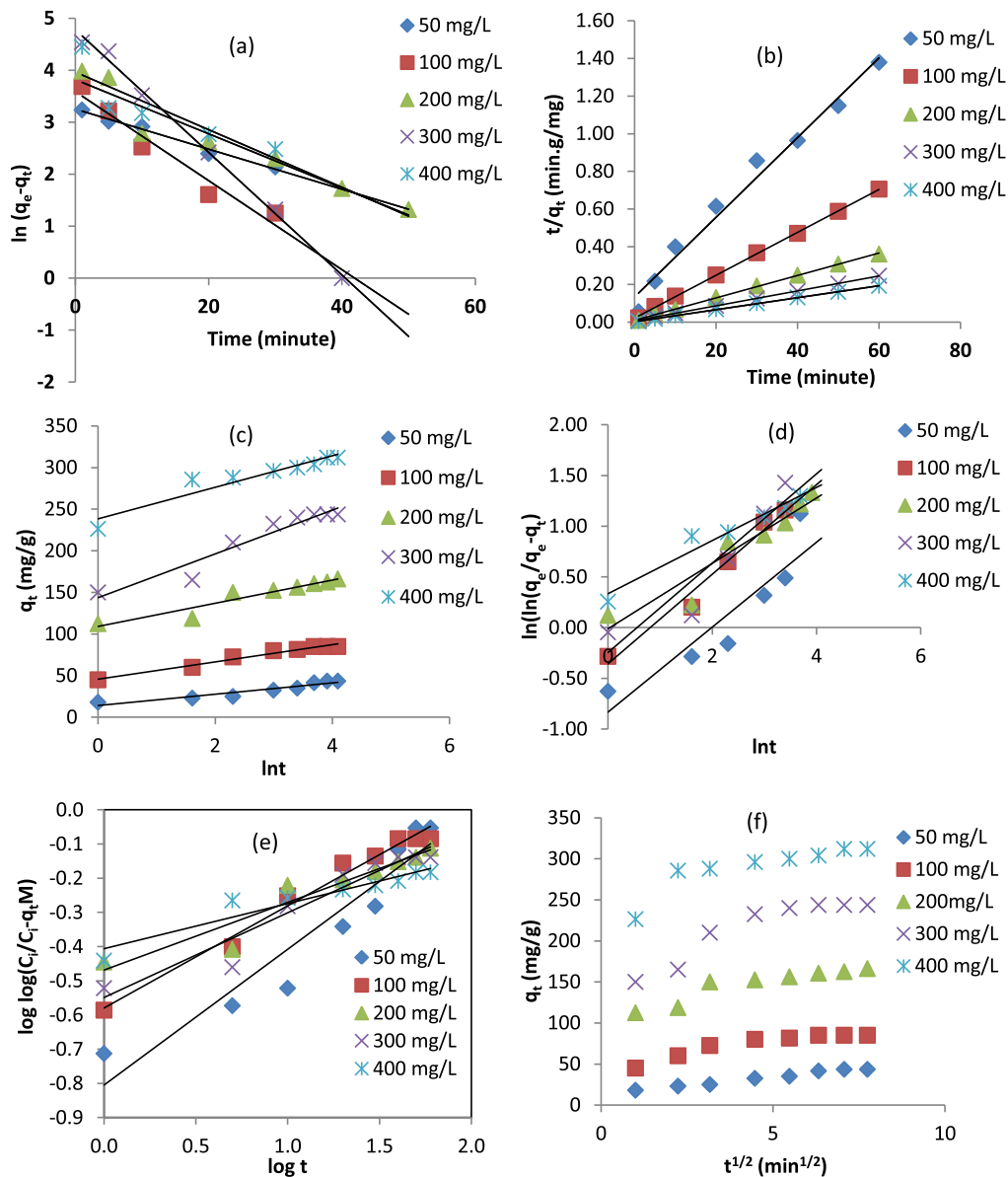


**Fig. 8.** Pseudo first order plots for uptake of RhB onto RH (a), Pseudo second order plots for uptake of RhB onto RH (b), Elovich plots for uptake of RhB onto RH (c), Avrami plots for uptake of RhB onto RH (d), Bangham model plots for uptake of RhB onto RH (e) and Intraparticle diffusion model plots for uptake of RhB onto RH (f).

**Table 7**  
Thermodynamics parameters for the adsorption of RhB onto RH.

Adsorbents	$\Delta H^\circ$ (KJ/mol)	$\Delta S^\circ$ (J/mol/K)	$\Delta G^\circ$ (KJ/mol)			
			303	313	323	333
RH	11.74	49.23	−3.122	−3.746	−4.257	−4.619

randomness at the solid-liquid interface could result from the higher translational entropy acquired by the displaced water molecules as compared to that lost as a result of dye uptake.  $\Delta H^\circ$  values obtained for the uptake of RhB onto RH was also found to be less than 40 kJ/mol, this further indicates physical adsorption for RH-RhB system.  $\Delta G^\circ$  values obtained were negative (Table 6) suggesting spontaneity of the adsorption process, higher negative values were obtained at higher temperature suggesting that adsorption process at higher temperature was more spontaneous.

### 3.9. Desorption studies

Desorption efficiencies were generally low ( $< 25\%$ ),  $\text{H}_2\text{O}$  was obtained to have the best desorption efficiency, desorption efficiency follows the order  $\text{H}_2\text{O} > \text{HCl} > \text{CH}_3\text{COOH}$  for the RH-RhB system. Desorption efficiency obtained for RH were 23.81%, 7.94% and 6.35% for  $\text{H}_2\text{O}$ , HCl and  $\text{CH}_3\text{COOH}$  respectively. This result further affirms that uptake of RhB onto RH is via physisorption. Low percentage desorption of RhB from RH surface may be attributed to a possibility of large net adsorption energy because of several contact points between large dye molecules and biosorbents [40].

### 3.10. Cost analysis

RH is a waste thus readily available at no cost, however the cost of transportation for its collection, water and energy for processing would amount to 0.021 USD/kg (21 USD/ton). Comparing the cost of RH with previous report, chemical activation of readily available adsorbent may result into about 24 times increase in cost while commercial activated carbon is about 1143 times more expensive than RH [41]. Thus RH gives a good economic advantage over modified adsorbents and commercial activated carbon.

## 4. Conclusion

RH was found to be effective in the uptake of RhB. Optimum adsorption was obtained at pH 3, RhB percentage removal rose up to 88.88% for adsorbent dosage of 2 g/L. Freundlich isotherm best describe the adsorption of RhB onto RH suggesting that adsorption was onto a non-uniform site. However initial rapid adsorption was onto a uniform site thus maximum monolayer adsorption capacity was obtained to be 666.67 mg/g. Adsorption energy (E),  $\Delta H^\circ$  and desorption studies suggests that the uptake of RhB onto RH was physical in nature. Elovich, Fraction power, Bangham and intraparticle diffusion models suggests that more than one mechanism was involved in the uptake of RhB onto RH.

## References

- [1] E.W. de Menezes, E.C. Lima, B. Royer, F.E. de Souza, B.D. dos Santos, J.R. Gregório, T.M.H. Costa, Y. Gushikem, E.V. Benvenutti, Ionic silica based hybrid material containing the pyridinium group used as an adsorbent for textile dye, *J. Colloid Interface Sci.* 378 (2012) 10–20.
- [2] R. Slimani, et al., Calcined eggshells as a new biosorbent to remove basic dye from aqueous solutions: thermodynamics, kinetics, isotherms and error analysis, *J. Taiwan Inst. Chem. Eng.* (2013). <http://dx.doi.org/10.1016/j.jtice.2013.10.009>.
- [3] H. Yemendzhiev, Z. Alexieva, A. Krastanov, Decolorization of synthetic dye reactive blue 4 by mycelial culture of white-rot fungi *trametes versicolor* 1, *Biotechnol. Biotechnol. Equip.* 23 (3) (2009) 1337–1339.
- [4] I. Anastopoulos, G.Z. Kyzas, Composts as biosorbents for decontamination of various pollutants: a review, *Water Air Soil Pollut.* 226 (2015) 61, <http://dx.doi.org/10.1007/s11270-015-2345-2>.
- [5] I.A.W. Tan, A.L. Ahmad, B.H. Hameed, Preparation of activated carbon from coconut husk: Optimization study on removal of 2,4,6-trichlorophenol using response surface methodology, *J. Hazard. Mater.* 153 (2008) 709–717.
- [6] Z. Wenxuan, L. Haijiang, K. Xiaowei, D. Lei, Y. Han, J. Ziwen, Y. Hu, L. Aimin, C. Rongshi, Adsorption of anionic dyes from aqueous solutions using chemically modified straw, *Bioresour. Technol.* 117 (2012) 40–47.
- [7] N.F. Cardoso, E.C. Lima, I.S. Pinto, C.V. Amavisca, B. Royer, R.B. Pinto, W.S. Alencar, S.F.P. Pereira, Application of cupuassu shell as biosorbent for the removal of textile dyes from aqueous solution, *J. Environ. Manag.* 92 (2011) 1237–1247.
- [8] N.F. Cardoso, R.B. Pinto, E.C. Lima, C. Calvete, C.V. Amavisca, B. Royer, M.L. Cunha, T.H.M. Fernandes, I.S. Pinto, Removal of remazol black B textile dye from aqueous solution by adsorption, *Desalination* 269 (2011) 92–103.
- [9] O.S. Bello, M. Auta, O.B. Ayodele, Ackee apple (*Blighiasapida*) seeds: a novel adsorbent for the removal of Congo Red dye from aqueous solutions, *Chem. Ecol.* <http://dx.doi.org/10.1080/02757540.2012.686606>.
- [10] M.C. Somasekhara, R.V. Nirmala, C. Ashwini, Bengal gram seed husk as an adsorbent for the removal of dyes from aqueous solutions – batch studies, *Arab. J. Chem.* <http://dx.doi.org/10.1016/j.arabjc.2013.09.029>.
- [11] V.M. Vučurović, R.N. Razmovski, U.D. Miljić, V.S. Puškaš, Removal of cationic and anionic azo dyes from aqueous solutions by adsorption on maize stem tissue, *J. Taiwan Inst. Chem. Eng.* 45 (2014) 1700–1708.
- [12] A.A. Inyinbor, F.A. Adekola, G.A. Olatunji, Adsorption of rhodamine B dye from aqueous solution on *Irvingia gabonensis* biomass: kinetics and thermodynamics studies, *S. Afr. J. Chem.* 68 (2015) 115–125.
- [13] O.S. Bello, M.A. Ahmad, Coconut (*Cocos nucifera*) shell based activated carbon for the removal of malachite green dye from aqueous solutions, *Sep. Sci. Technol.* 47 (6) (2012) 903–912.
- [14] B.H. Hameed, D.K. Mahmoud, A.L. Ahmad, Equilibrium modeling and kinetic studies on the adsorption of basic dye by a low-cost adsorbent: coconut (*Cocos nucifera*) bunch waste, *J. Hazard. Mater.* 158 (2008) 65–72.
- [15] R.H. Hesas, A. Arami-Niya, Wan Mohd Ashri Wan Daud, J.N. Sahu, Preparation of granular activated carbon from oil palm shell by microwave-induced chemical activation: optimisation using surface response methodology, *Chem. Eng. Res. Des.* 9 (1) (2013) 2447–2456.
- [16] A.M. Aljeboree, A.N. Alshirifi, Ayad F. Alkaim, Kinetics and equilibrium study for the adsorption of textile dyes on coconut shell activated carbon, *Arab. J. Chem.* <http://dx.doi.org/10.1016/j.arabjc.2014.01.020>.
- [17] A. Kundu, B.S.M.A. Gupta, M.A. Hashim, G. Redzwan, Taguchi optimization approach for production of activated carbon from phosphoric acid impregnated palm kernel shell by microwave heating, *J. Clean. Prod.* 105 (2015) 420–427.
- [18] H.D. Setiabudi, R. Jusoh, S.F.R.M. Suhaimi, S.F. Masrur, Adsorption of methylene blue onto oil palm (*Elaeis guineensis*) leaves: process optimization, isotherm, kinetics and thermodynamic studies, *J. Taiwan Inst. Chem. Eng.* 63 (2016) 363–370.
- [19] G.Z. Kyzas, D.N. Bikaris, Recent modifications of chitosan for adsorption applications: a critical and systematic review, *Mar. Drugs* 13 (2015) 312–337, <http://dx.doi.org/10.3390/md13010312>.
- [20] G.Z. Kyzas, K.A. Matis, Nanoadsorbents for pollutants removal: a review, *J. Mol. Liq.* 203 (2015) 59–168.
- [21] I. Langmuir, The constitutional and fundamental properties of solids and liquids, *J. Am. Chem. Soc.* 38 (1916) 2221–2295.
- [22] H.M.F. Freundlich, Over the adsorption in solution, *Z. Phys. Chem.* 57 (1906) 385–470.

- [23] M.M. Dubinin, L.V. Radushkevich, Equation of the characteristic curve of activated charcoal, *Proc. Acad. Sci. Phys. Chem. USSR* 55 (1947) 331–333.
- [24] M.I. Temkin, V. Pyzhev, Kinetics of ammonia synthesis on promoted iron catalyst, *Acta USSR* 12 (1940) 327–356.
- [25] I. Anastopoulos, G.Z. Kyzas, Agricultural peels for dye adsorption: a review of recent literature, *J. Mol. Liq.* 200 (2014) 381–389.
- [26] S. Lagergren, B.K. Svenska, On the theory of so-called adsorption of materials, *R. Swed. Acad. Sci. Doc Band* 24 (1898) 1–13.
- [27] Y.S. Ho, G. McKay, Pseudo-second order model for sorption processes, *Proc. Biochem.* 34 (1999) 451–465.
- [28] C. Aharoni, M. Ungarish, Kinetics of activated chemisorptions. Part I: the non-Elovichian part of the isotherm, *J. Chem. Soc. Faraday Trans.* 72 (1976) 265–268.
- [29] M. Avrami, Kinetics of phase change: transformation-time relations for random distribution of nuclei, *J. Chem. Phys.* 8 (1940) 212–224.
- [30] W.J. Weber, J.C. Morris, Kinetics of adsorption on carbon from solution, *J. Sanitary Eng. Div. Am. Soc. Civil Eng.* 89 (1963) 31–59.
- [31] A.A. Inyinbor, F.A. Adekola, G.A. Olatunji, EDTA modified *Irvingia gabonensis*: an efficient bioresource material for the removal of rhodamine B, *Pakistan J. Anal. Environ. Chem.* 16 (2) (2015) 38–45.
- [32] A.A. Inyinbor, F.A. Adekola, G.A. Olatunji, Liquid phase adsorptions of rhodamine B dye onto raw and chitosan supported mesoporous adsorbents: isotherms and kinetics studies, *Appl. Water Sci.* (2016) 1–11, <http://dx.doi.org/10.1007/s13201-016-0405-4>, <http://link.springer.com/article/10.1007/s13201-016-0405-4>.
- [33] K. Shakir, A.F. Elkafrawy, H.F. Ghoneimy, S.G.E. Beheir, M. Refaat, Removal of rhodamine B a basic dye and thoron an acidic dye from dilute aqueous solutions and wastewater simulants by ion flotation water research, *Water Res.* 44 (2010) 1449–1461.
- [34] K.G. Bhattacharyya, S. SenGupta, G.K. Sarma, Interactions of the dye, rhodamine B with kaolinite and montmorillonite in water, *Appl. Clay Sci.* 99 (2014) 7–17.
- [35] M.V. Sureshkumar, C. Namasivayam, Adsorption behavior of direct red 12B and rhodamine B from water unto surfactant-modified coconut coir pith, *Colloid Surf. A: Physicochem. Eng. Asp.* 317 (1–3) (2008) 277–283.
- [36] J. Yu, B. Li, X. Sun, Y. Jun, R. Chi, Adsorption of methylene blue and rhodamine B on baker's yeast and photocatalytic regeneration of the biosorbent, *Biochem. Eng. J.* 45 (2009) 145–151.
- [37] Z. Zhang, Ian M. O'Hara, Geoff A. Kent, William O.S. Doherty, Comparative study on adsorption of two cationic dyes by milled sugarcane bagasse, *Ind. Crop. Prod.* 42 (2013) 41–49.
- [38] M. Zamouche, O. Hamdaoui, Sorption of rhodamine B by cedar cone: effect of pH and ionic strength, *Energy Procedia* 18 (2012) 1228–1239.
- [39] M.A. Ahmad, N. Ahmad, O.S. Bello, Removal of remazol brilliant blue reactive dye from aqueous solutions using watermelon rinds as adsorbent, *J. Dispers. Sci. Technol.* 36 (6) (2015) 845–858, <http://dx.doi.org/10.1080/01932691.2014.925400>.
- [40] M.E. Fernandez, G.V. Nunell, P.R. Bonelli, A.L. Cukierman, Effectiveness of *Cupressus sempervirens* cones as biosorbent for the removal of basic dyes from aqueous solutions in batch and dynamic modes, *Bioresour. Technol.* 101 (2010) 9500–9507.
- [41] O.S. Bello, M.A. Ahmad, Response surface modeling and optimization of remazol brilliant blue reactive dye removal using periwinkle shell-based activated carbon, *Sep. Sci. Technol.* 46 (15) (2011) 2367–2379.